ELSEVIER

Physica A 306 (2002) 199–210

PHYSICA A

www.elsevier.com/locate/physa

Phase front dynamics in inhomogeneously forced oscillatory systems

Christopher Hemming, Raymond Kapral*

Chemical Physics Theory Group, Department of Chemistry, University of Toronto, Toronto, Ont., Canada M5S 3H6

Abstract

Resonantly forced reaction–diffusion systems possess phase-locked domains separated by phase fronts. A nonequilibrium Ising–Bloch bifurcation in which a stationary Ising front loses stability to a pair of counterpropagating Bloch fronts with opposite chirality exists in 2:1 forced systems. For such systems, we study the effects of a spatially inhomogeneous forcing intensity which varies in space across the bifurcation. In such a case, a propagating Bloch front which encounters a domain where the forcing intensity lies in the Ising regime undergoes a change in chirality and is reflected from the Ising domain. This phenomenon is studied analytically and numerically in one dimension. In two dimensions systems with regular and disordered forcing are studied; the spatial arrangement of Ising domains may give rise to complex pattern dynamics.

1. Introduction

Reaction–diffusion systems in the far-from-equilibrium domain show a diversity of spatio-temporal regular and chaotic patterns. An especially interesting class of such systems is oscillatory reaction–diffusion media which are resonantly forced by an external periodic driving field. The external forcing may resonantly lock the dynamics yielding phase-locked states that are complicated spatiotemporal analogs of the phase-locked states seen in simpler ordinary differential equation systems. These resonant patterns typically involve the existence of spatial domains of phase-locked regions with different oscillation phases separated by fronts in which the phase changes rapidly between two locked values. The number of different types of phase-locked regions depends on the frequency and amplitude of the forcing relative to that of the underlying oscillation of the system. More specifically, if the unforced spatially homogeneous system has period

* Corresponding author. Tel.: +1-416-978-6106; fax: +1-416-978-5325.
E-mail address: rkapral@gatto.chem.utoronto.ca (R. Kapral).

0378-4371/02/$ - see front matter
PII: S0378-4371(02)00498-3

$T_0 = 2\pi/\omega_0$ and the ratio of the forcing frequency ω_f to ω_0 is sufficiently close to a rational ratio of integers, $\omega_f/\omega_0 \approx n/m$, for a strong enough forcing amplitude the system's oscillatory dynamics may become entrained to the external forcing. In this case the system possesses n stable limit cycle solutions with periods $T = nT_f = 2n\pi/\omega_f \approx mT_0$ which are mapped into each other under phase shifts $t \to t + kT/n$ for $k = 0, 1, 2, \ldots$. The geometry of these phase-locked zones may be complex and different types of chemical patterns can result from transverse instabilities of the phase fronts separating the domains. Such patterns have been observed experimentally in the resonantly forced light-sensitive Belousov–Zhabotinsky reaction [1–5].

Spatial inhomogeneities in reaction–diffusion systems can bring about qualitative changes in the pattern dynamics and are obviously of relevance since many naturally occurring reaction–diffusion processes take place in media that are spatially inhomogenous. In the present context, if the external forcing is spatially inhomogeneous, new phase locking phenomena appear. In experiments on reaction–diffusion systems such inhomogeneous forcing can be realized by using light sources tailored to yield the desired pattern of illumination. Wave propagation processes for random inhomogeneous 3:1 resonantly forced systems were studied earlier and phenomena such as phase front roughening, pulse and compound front formation and their effects on spiral wave dynamics were explored [6].

In this paper we study 2:1 resonantly forced systems with specific regular and random patterns of inhomogeneous forcing where new phenomena appear. Rather than focusing on a specific reaction–diffusion system, in these studies we employ the forced complex Ginzburg–Landau (FCGL) equation

$$\frac{\partial}{\partial t} A(\mathbf{r}, t) = (\mu + \mathrm{i}\nu)A - (1 + \mathrm{i}\beta)|A|^2 A + \gamma(\mathbf{r})\bar{A} + (1 + \mathrm{i}\alpha)\nabla^2 A \,. \tag{1}$$

Eq. (1) is the normal form of the Hopf bifurcation for a diffusively coupled field of nonlinear oscillators subject to external periodic forcing at the 2:1 subharmonic resonance [7,8]. The quantity $A(\mathbf{r}, t)$ is a complex amplitude describing the envelope of the oscillations and $\bar{A}$ is its complex conjugate. For 2:1 forcing, when $\gamma > \gamma_c = |\nu - \beta\mu|/\sqrt{1 + \beta^2}$ there are two phase-locked states which differ in phase by π, determined from the fixed point solutions of Eq. (1), corresponding to the two limit cycle solutions of the underlying reaction–diffusion system. We assume that the forcing intensity $\gamma(\mathbf{r})$ depends on position. In addition to providing a generic description of reaction–diffusion dynamics in the vicinity of a Hopf bifurcation, Eq. (1) appears in optics and in the description of liquid crystals in the presence of magnetic fields [9–11].

For $\gamma > \gamma_c$, the one-dimensional form of Eq. (1) exhibits front solutions between spatially uniform domains in which A takes one of two values corresponding to stable phase-locked states. There is a stationary front solution, called the Ising front, which is invariant under the transformation $(A, x) \to (-A, -x)$. There exists a bifurcation in which the Ising front loses stability and a pair of stable front solutions travelling in opposite directions emerge; taking the front velocity c as the order parameter, this is a pitchfork bifurcation known as the nonequilibrium Ising–Bloch (NIB) bifurcation (see Fig. 1) [12]. The parameter $\chi \equiv \sigma|A(s)|$ associated with a front, where s is the front position and $\sigma = \pm 1$ for the two Bloch fronts, is also useful as an order parameter (see

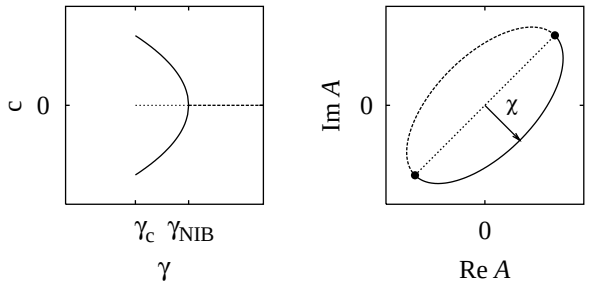

Fig. 1. Left: schematic bifurcation diagram for the nonequilibrium Ising–Bloch bifurcation in the 2:1 FCGL equation. Front velocity c is plotted against γ. The Bloch front solutions are indicated by solid curves, the Ising front is shown by long dashes where it is stable and by short dashes where it is unstable. Below γ_c there are no front solutions because the system is not phase-locked. Right: a pair of Bloch front solutions (solid line, long dashes) and an Ising front solution (short dashes) plotted in the complex A-plane. The two solid dots represent the phase-locked states. The arrow indicates graphically the parameter χ for the Bloch front that is plotted in solid line.

Fig. 1(b)). The presence of an NIB bifurcation in the 2:1 FCGL equation suggests that it is a generic feature of 2:1 resonantly forced oscillatory media, and indeed it has been found in a wide variety of such systems, both theoretical and experimental, as well as in bistable reaction–diffusion systems [11,10,13–17]. In the general case the two stationary states are not equivalent and the pitchfork unfolds to a limit-point bifurcation. In systems near the NIB bifurcation, perturbations may drive the front from one Bloch solution branch to the other, thereby causing a front reversal. Reversals due to front curvature, advective fields and boundary effects have been studied [15–20].

In this paper we consider the NIB bifurcation with spatially inhomogeneous forcing where there are important effects on the nature and dynamics of the Ising or Bloch fronts that separate phase-locked domains. In particular, if the forcing parameter varies locally from values that support Ising fronts to values that support Bloch fronts the character of the dynamics and pattern formation processes will be strongly influenced.

2. Front reversals in one dimension

Consider a simple one-dimensional situation where $\gamma(x) = \gamma_{\mathrm{NIB}} + b(x - x_0)$ varies linearly with position. For $\gamma(x) \leqslant \gamma_{\mathrm{NIB}}$ the system supports Bloch fronts while for $\gamma > \gamma_{\mathrm{NIB}}$ it supports Ising fronts. Further, suppose the two phase-locked states are equivalent so that the Ising front is stationary in the homogeneous system. Given this situation, one may initiate a Bloch front in the spatial domain $x < x_0$ which travels to the right (increasing x). Fig. 2(a) shows that the Bloch front propagates to the right for a certain distance at which point it is reflected and a Bloch front with opposite parity travelling in the opposite direction is produced. Except where stated otherwise, numerical simulations were conducted with the parameter values $\mu=1$, $\nu=0.1$, $\alpha=-0.1$,

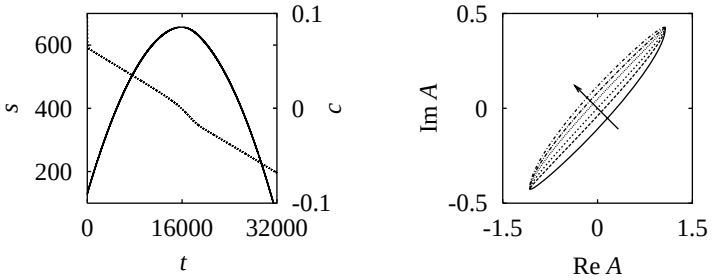

Fig. 2. Left: plot of $s(t)$ (solid line, left axis) and $c = \dot{s}(t)$ (dashes, right axis) for a Bloch front travelling in a system in which $\gamma(x)$ varies linearly with x across the NIB bifurcation, $\gamma(x) = \gamma_{\mathrm{NIB}} + b(x - x_0)$, with $b = 8 \times 10^{-6}$ and $x_0 = 668.498$. Right: plot of $A(x,t)$ in the A-plane at various times during the simulation. The solid curve corresponds to $t = 1000$; subsequent curves are taken at later times at intervals of $\Delta t = 5000$. The arrow indicates the direction of increasing time.

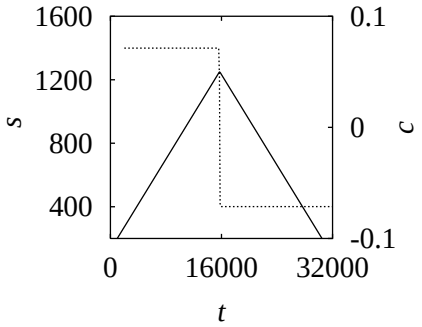

Fig. 3. Plot of $s(t)$ (solid line, left axis) and $c(t)$ (dashed line, right axis) for a Bloch front travelling in a system in which $\gamma(x)$ is a step function between Bloch and Ising domains, $\gamma(x) = \gamma_{\mathrm{I}}\theta(x - x_0) + \gamma_{\mathrm{B}}\theta(x_0 - x)$, where θ is the Heaviside function, $\gamma_{\mathrm{B}} = 0.43$, $\gamma_{\mathrm{I}} = 0.44$ and $x_0 = 1250.125$.

$\beta = -0.15$, for which $\gamma_c \simeq 0.2472$ and $\gamma_{\mathrm{NIB}} \simeq 0.4353$.[1] The change in the Bloch front type is demonstrated in Fig. 2(b) by the change in the sign of χ with time. Since χ passes through zero the conversion between the two Bloch fronts occurs by passage through an Ising front. A similar phenomenon occurs in the case where $\gamma(x)$ is a step function defining distinct Bloch and Ising domains. In a simulation with $\gamma(x) = \gamma_{\mathrm{I}}\theta(x - x_0) + \gamma_{\mathrm{B}}\theta(x_0 - x)$, where $\gamma_c < \gamma_{\mathrm{B}} < \gamma_{\mathrm{NIB}}$ and $\gamma_{\mathrm{I}} > \gamma_{\mathrm{NIB}}$, and $\theta(x)$ is the Heaviside function, we observe a front reversal which takes place on a length scale on the order of the front width (see Fig. 3). This case is a model for the $\gamma(\mathbf{r})$ field in the two-dimensional disk studies discussed in Section 3 where the $\gamma(\mathbf{r})$ field is discontinuous at the boundary between the Ising and Bloch regions.

[1] Numerical integrations were performed using explicit forward differencing with discretization step sizes $\Delta x = 0.25$, $\Delta t = 0.01$ or $\Delta x = 1$, $\Delta t = 0.02$. In two-dimensions a nine point discrete Laplacian with fourth-order accuracy was used.

For spatially uniform forcing Eq. (1) possesses travelling front solutions $A(x,t) = A(x-ct)$ which satisfy

$$(\mu + \mathrm{i}\nu)A - (1+\mathrm{i}\beta)|A|^2 A + \gamma\bar{A} + c\,\frac{\partial}{\partial x}A + (1+\mathrm{i}\alpha)\,\frac{\partial^2}{\partial x^2}A = 0\,. \tag{2}$$

When the parameters ν, α, β are all zero, then Eq. (1) may be written in variational form as

$$\frac{\partial}{\partial t}A(x,t) = -\frac{\delta\mathscr{F}[A,\bar{A}]}{\delta\bar{A}}\,, \tag{3}$$

where the functional $\mathscr{F}[A,\bar{A}]$ is given by

$$\mathscr{F}[A,\bar{A}] = \int_{-\infty}^{+\infty} \mathrm{d}x \left\{ -\mu|A(x)|^2 + \frac{|A(x)|^4}{2} - \frac{\gamma}{2}(\bar{A}^2 + A^2) + \left|\frac{\partial A(x)}{\partial x}\right|^2 \right\}\,. \tag{4}$$

In this spatially uniform variational case, one may find exact analytic expressions for the Bloch and Ising front solutions. Writing these as $A_0 = X_0 + \mathrm{i}Y_0$, the complementary pair of Bloch fronts is

$$X_0 = \sqrt{\mu+\gamma}\tanh(x\sqrt{2\gamma})\,,$$

$$Y_0 = \pm\,\frac{\sqrt{\mu-3\gamma}}{\cosh(x\sqrt{2\gamma})}\,. \tag{5}$$

and the Ising front is

$$X_0 = (\mu+\gamma)^{1/2}\tanh\left[\left(\frac{\mu+\gamma}{2}\right)^{1/2}x\right]\,,$$

$$Y_0 = 0. \tag{6}$$

It is a consequence of the variational property of the system that both the Ising and Bloch fronts have zero velocity.

While it is difficult to examine the front reversal phenomenon analytically for general parameter values and arbitrary forms of the spatial variation of $\gamma(x)$, one may gain insight into its origin by studying systems near the variational limit with small gradients in the γ field. Coullet et al. derived the form of the NIB bifurcation by considering a perturbation about the variational case in which the nonvariational parameters α, β and ν are of order ε [12]. We extend their approach by taking $\gamma(x)$ to vary linearly in space with $\gamma' = \mathrm{d}\gamma(x)/\mathrm{d}x \sim \mathscr{O}(\varepsilon)$.

We expand in ε about the variational and spatially uniform front solution A_0, evaluated for $\gamma \equiv \gamma(s)$, where $\gamma(s)$ is the value of $\gamma(x)$ at the front position s. As the front travels, the zeroth order solution A_0 will change in time, however, since both γ' and the front velocity $c = \dot{s}$ are of order ε, the lowest order at which terms arising from the front motion will appear is $\mathscr{O}(\varepsilon^2)$. We make a coordinate change to the moving frame $\zeta = x - s(t^*) - \varepsilon\dot{s}(t)(t-t^*)$ which has the same instantaneous velocity as the front at the arbitrary reference time t^*. Writing the front as $A = A_0 + \varepsilon a + \mathscr{O}(\varepsilon^2)$, and

substituting this form into Eq. (2), we obtain

$$(\mu + \mathrm{i}\varepsilon v)(A_0 + \varepsilon a) - (1 + \mathrm{i}\varepsilon\beta)(A_0 + \varepsilon a)^2(\bar{A}_0 + \varepsilon\bar{a}) + \varepsilon\dot{s}(A_{0\zeta} + \varepsilon a_\zeta) + (\gamma(s) + \varepsilon\gamma'(s)\zeta)(\bar{A}_0 + \varepsilon\bar{a}) + (1 + \mathrm{i}\varepsilon\alpha)(A_{0\zeta\zeta} + \varepsilon a_{\zeta\zeta}) + O(\varepsilon^2) = O(\varepsilon^2)\,. \tag{7}$$

At order ε we obtain the linear equation in $a = [a_r\ a_i]^{\mathrm{T}}$,

$$(1 - 2|A_0|^2 + \partial_{\zeta\zeta})a + (\gamma(s) - A_0^2)\bar{a} = -\mathrm{i}vA_0 + \mathrm{i}\beta|A_0|^2A_0 - \mathrm{i}\alpha A_{0\zeta\zeta} - cA_{0\zeta} - \gamma'(s)\zeta\bar{A}_0\,. \tag{8}$$

The zero eigenvector of the adjoint of the linear operator on the left-hand side of Eq. (8) is $[X_{0\zeta}\ Y_{0\zeta}]$. Applying the solvability condition to this equation and using the Bloch front solutions Eq. (5) for A_0 we obtain

$$\dot{s} = -\frac{3\gamma'(s)(\mu - \gamma(s))}{2\gamma(s)(3\mu - \gamma(s))} \pm \left(\frac{(\mu + \gamma(s))(\mu - 3\gamma(s))}{2\gamma(s)}\right)^{1/2} \frac{3\pi((\alpha - \beta)\gamma(s) + \beta\mu - v)}{2(3\mu - \gamma(s))} \tag{9}$$

as the equation of motion for the front position s. This equation is the same as that obtained by Coullet et al. for the spatially uniform γ case [12], except for the $-3\gamma'(s)(\mu - \gamma(s))/(2(3\mu - \gamma(s)))$ term which appears because of the gradient in γ. This term gives rise to a difference in the speed of the two counter-propagating Bloch fronts; the front moving up the gradient in γ does not have the same speed as the one moving down the gradient. The same analysis may be performed for the Ising front, using the variational solution Eq. (6), and we find

$$\dot{s} = \frac{-3\gamma'(s)}{2(\mu + \gamma(s))}\,. \tag{10}$$

As in the spatially uniform case, we obtain from Eq. (9) that $\gamma_{\mathrm{NIB}} = \mu/3$. The front velocity at the bifurcation, $\dot{s}(\gamma_{\mathrm{NIB}}) = -9\gamma'/8$. Unlike the spatially uniform case, the Ising front possesses a nonzero velocity when γ varies spatially. Eq. (10) predicts that the Ising front will move toward lower γ and thus will eventually be expelled from the Ising region in the case of linearly ramped $\gamma(x)$. The terms arising from the spatial dependence of γ are independent of the nonvariational parameters v, β and α, and therefore are a feature of the variational system.

A comparison of the velocity relations Eqs. (9) and (10) for the case $\gamma' \neq 0$ with the spatially uniform $\gamma' = 0$ case is shown in Fig. 4 (left panel). The spatially varying γ case possesses a stable fixed point on the upper Bloch branch, indicated by a dot. Thus, the analysis predicts that an ingoing Bloch front will become pinned near the Ising–Bloch boundary rather than reflect, which is in contrast to the numerical simulation result for a system far from the variational regime. The front reversal for systems well into the nonvariational regime arises from the breakdown of the perturbation approximation. In simulations with smaller nonvariational parameters, the results agree with the predictions of the perturbation calculation. Fig. 4 (right panel) shows front

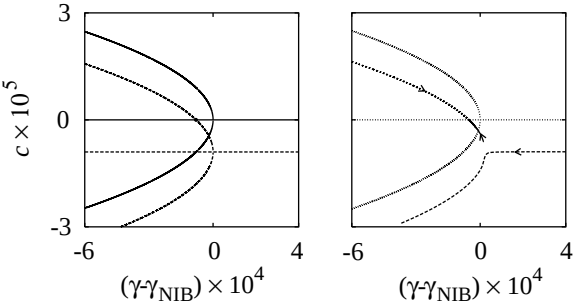

Fig. 4. Left: the c–γ relation of Eqs. (9) and (10) for $\gamma' = 0$ (solid line) and $\gamma' = 8 \times 10^{-6}$ (dashed line). The dot indicates the stable fixed point of Eq. (9). The constant $\gamma_{NIB} = 1/3$. Right: dependence of c on γ measured in numerical simulations of Eq. (1) in systems with spatially uniform γ (dotted line). The other curves in the right panel are $c(s)$ versus $\gamma(s)$ in a system in which γ varies linearly with spatial gradient $\gamma' = 8 \times 10^{-6}$, from various initial conditions. The constant $\gamma_{NIB} = 0.33278472$. In all the cases in both panels the other parameters are $\mu = 1$, $\nu = 1 \times 10^{-4}$, $\alpha = -1 \times 10^{-4}$ and $\beta = -1.5 \times 10^{-4}$.

trajectories from three simulations. In these an ingoing Bloch front becomes pinned, a Bloch front of the same sign started between the fixed point and the Ising–Bloch boundary travels outward and becomes pinned at the same point, and a front well inside the Ising region travels out of the region, emerging on the lower Bloch front branch of the pitchfork. The agreement between the numerical simulation results and Eqs. (9) and (10) is evident.

3. Regular arrays of disks

In two spatial dimensions Bloch front reversals may lead to more complex dynamics. We suppose that the $\gamma(\mathbf{r})$ field takes a value $\gamma = \gamma_B$ that lies within the Bloch regime at all spatial points, except for $\mathbf{r}$ values within a collection of disks where $\gamma = \gamma_I$, and γ_I is in the Ising regime ("Ising disks"). More specifically, the $\gamma(\mathbf{r})$ fields we consider are of the form

$$\gamma(\mathbf{r}) = \begin{cases} \gamma_I & \text{if } |\mathbf{r} - \mathbf{r}_i| < R, \ \ i \in 1, 2, \ldots, N\,, \\ \gamma_B & \text{otherwise}\,, \end{cases} \tag{11}$$

where $\mathbf{r}_i$, $i = 1, 2, \ldots, N$ are the centers of the Ising disks, R is the disk radius, γ_B satisfies $\gamma_c < \gamma_B < \gamma_{NIB}$ with γ_c the γ value below which phase locking does not occur, and $\gamma_I > \gamma_{NIB}$. Diverse wave patterns can arise from the interaction of Bloch fronts with Ising obstacles and we give several examples of such dynamics below. In the studies described in this section, $\gamma_B = 0.4$ and $\gamma_I = 0.5$.

Suppose a Bloch front strikes a single Ising disk. In Fig. 5 we see that the front wraps around the disk and reconnects on the other side of it. The result is two structures: the original front, which passes through undisturbed (apart from the transient associated with striking the disk), and an expanding, ultimately circular wavefront which is formed

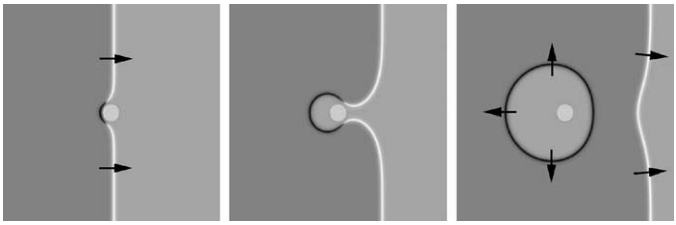

Fig. 5. A planar front, travelling to the right in a Bloch medium, incident on a single Ising disk of radius $R = 7.5$. Boundary conditions are periodic on the top and bottom sides and no-flux on the left and right sides; the system size is 200×200. Time increases from left to right in units of 200. For all figures in this section: (i) the phase field is shown using a nonlinear gray scale chosen to color the two types of Bloch fronts black or white and the phase-locked states in the two medium gray shades; (ii) the circular disks indicate where $\gamma(\mathbf{r}) = \gamma_{\mathrm{I}}$, everywhere else $\gamma(\mathbf{r}) = \gamma_{\mathrm{B}}$; (iii) arrows indicate the direction of front propagation.

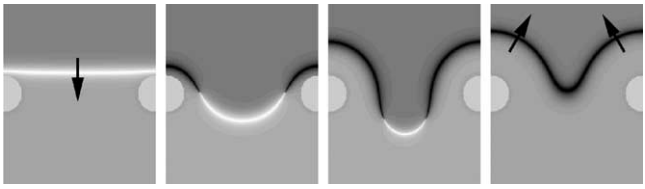

Fig. 6. A Bloch front incident on an Ising disk with radius $R = 5$ in a system with periodic boundary conditions on the left and right sides. On the top and bottom sides boundary conditions are no-flux. The system size is 62.5×100; the central portion with dimensions 62.5×50 is shown. From left to right, frames correspond to $t = 210$, 300, 420, 450.

from the reflected wave. The center of the expanding Bloch front does not lie on the center of the Ising disk but slightly in front of it. For a sufficiently small disk the front passes over the disk without wavefront reflection and hence no approximately circular wavefront is formed; the front experiences only a transient perturbation.

We next consider a planar Bloch front incident on a row of Ising disks, or equivalently, a single Ising disk with periodic boundary conditions at the edges perpendicular to the front. For sufficiently closely spaced disks, the incident front is unable to penetrate through the gap between the disks (Fig. 6). Wave blocks arising in similar geometries are common in excitable media [21], and may be explained in terms of effects due to wavefront curvature. Reaction–diffusion fronts typically obey a velocity–curvature relation of the form $c_n = c_p - \mathscr{D}\kappa$ where c_n is the normal front velocity, c_p is the planar front velocity, κ is the front curvature and $\mathscr{D}$ is a diffusion coefficient. Diffusion tends to reduce front curvature, which may be related to the gap size, and for sufficiently small gaps the front fails to propagate. For the Bloch fronts considered here an additional factor plays a role: the Bloch type in the central portion of the front. Between frames 3 and 4 of Fig. 6 (left to right) we see that the front has changed Bloch type but this reversal is not due to a collision with an Ising region. Systems are known where front curvature can induce a transition from one Bloch front branch to the other [15,18–20,16]; however, in the 2:1 FCGL equation at these parameters, a

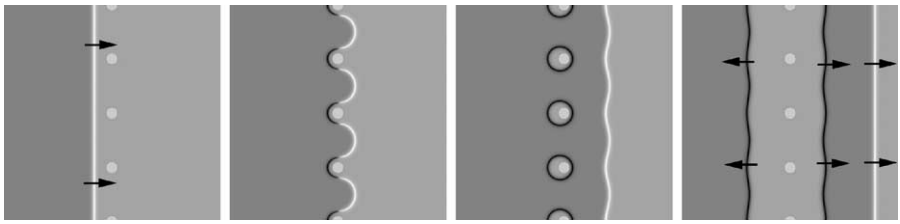

Fig. 7. A Bloch front incident on a row of Ising disks of radius $R = 5$ with centers separated by 50 space units. Time increases from left to right in units of 200. The initial front travels to the right. The net result of the interaction is one reflected front travelling to the left and two transmitted fronts travelling to the right. Boundary conditions are periodic on the top and bottom sides and no-flux on the left and right sides; the system size is 200×200.

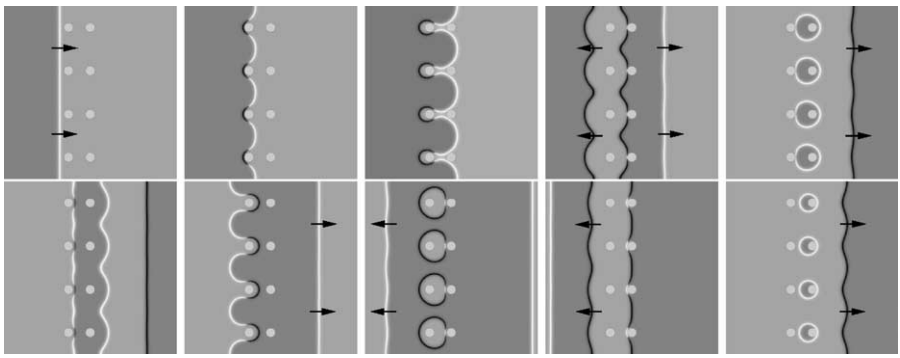

Fig. 8. A Bloch front incident from the left on two rows of Ising disks of radius $R = 5$. The vertical spacing between the centers of disks is 50, the horizontal spacing is 25. From left to right and top to bottom, the frames are taken at $t = 300$, 400, 600, 800, 1200, 1300, 1500, 1700, 1800, 2100. An oscillating configuration is obtained as a result of the fronts reflected between the two rows. In the time interval shown four fronts are emitted from the right-hand side of the structure and three are emitted from the left-hand side. Boundary conditions are periodic on the top and bottom sides and no-flux on the left and right sides; the system size is 200×200.

circular disk can shrink to extinction without such a transition occurring, implying that there is no critical curvature which forces a change in Bloch front type. The simulations show that the phase defects where the front changes Bloch type move along the front and eventually meet and annihilate.

Fig. 7 shows a system in which the disks are spaced slightly farther apart than those in Fig. 6. In this case the wavefront "tongues" penetrate through the disks and recombine, giving rise to a transmitted front and expanding approximately circular fronts. Far from the disks, the net outcome of a front collision with this structure is two transmitted plane fronts and a single reflected front.

For the case where there are two rows of disks, for certain spacings between them, an oscillating configuration may arise (Fig. 8). The front reflected when the wavefront strikes the second row of disks travels back to the first row, where it gives rise to a

transmitted wavefront and a reflected front. This process repeats, and an infinite train of fronts is emitted from each side. When the second row of disks is placed at a sufficiently large distance from the first, the fronts reflected from the second row of disks may annihilate upon collision with the second front transmitted through the first row, thus quenching the transmitted fronts.

4. Spatially random forcing fields

If the forcing field is a time-independent stochastic function of position new types of phase pattern dynamics are observed. As an example of such random forcing we consider a spatially dichotomous random forcing field: the system was divided into square domains of length ℓ on each of which γ was set equal to γ_1 with probability p and γ_2 with probability $q = 1 - p$. The spatial average value of γ is given by $\bar{\gamma} = p\gamma_1 + (1 - p)\gamma_2$ and it is interesting to see how the dynamics of the system with inhomogeneous forcing differs from that with uniform forcing at $\bar{\gamma}$. The dynamics depends on the sizes ℓ of the spatial domains within which γ is constant, the two values of γ, and the probability p. We considered two cases: (i) $\gamma_1 = 0.3$, within the Bloch regime and $\gamma_2 = 0.5$, within the Ising regime, and (ii) $\gamma_1 = 0$, below the phase-locking threshold γ_c and $\gamma_2 = 1$, within the Ising regime. Different values of $\bar{\gamma} = p\gamma_1 + (1 - p)\gamma_2$ were obtained by varying the probability p. In the work below we adjust p so that $\bar{\gamma} = 0.38$ for both cases (i) and (ii) and show that the dynamics is not determined solely by the mean field value $\bar{\gamma}$.

Fig. 9 shows dynamics for case (i) in a system with periodic boundary conditions from initial conditions containing two spatially uniform states separated by chiral planar fronts,

$$A(x, y, 0) = \begin{cases} \mathrm{i}A_0 & \text{if } 0 \leqslant x < w\,, \\ -A_0 & \text{if } w \leqslant x < L/2\,, \\ -\mathrm{i}A_0 & \text{if } L/2 \leqslant x < L/2 + w\,, \\ A_0 & \text{if } L/2 + w \leqslant x \leqslant L\,, \end{cases} \tag{12}$$

where A_0 is one of the phase-locked states for the uniform $\gamma = 0.38$ system. In a spatially uniform system with $\gamma \equiv 0.38$, this initial condition will give rise to two planar propagating Bloch fronts and no phase defects will be nucleated. In the spatially inhomogeneous case (i), a complex, irregular state with time-varying dynamics is obtained, and the initial pattern has been obliterated. The fronts are Bloch-like, there are many phase defects present, and there are many domain-splitting and front reversal events. A qualitative explanation of these effects is as follows: diffusion leads to some local averaging of the $\gamma(\mathbf{r})$ field, yielding a local effective $\bar{\gamma}(\mathbf{r})$ which varies between the Bloch and Ising regimes.[2] Hence, one has propagating Bloch fronts which reverse upon encountering Ising domains.

[2] A similar analysis was used for the 3:1 resonantly forced systems discussed in Ref. [6].

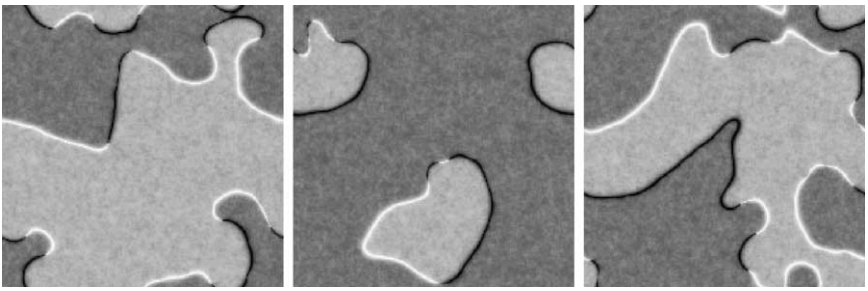

Fig. 9. Phase field of the 2:1 FCGL equation with $\gamma_1 = 0.3$, $\gamma_2 = 0.5$, $p = 0.6$, $\bar{\gamma} = 0.38$, $\ell = 1$ (order of the diffusion length), system size is 200×200, with periodic boundary conditions. Time increases from left to right in units of 1000 and results are shown after a transient time of $t_0 = 16\,000$ time units.

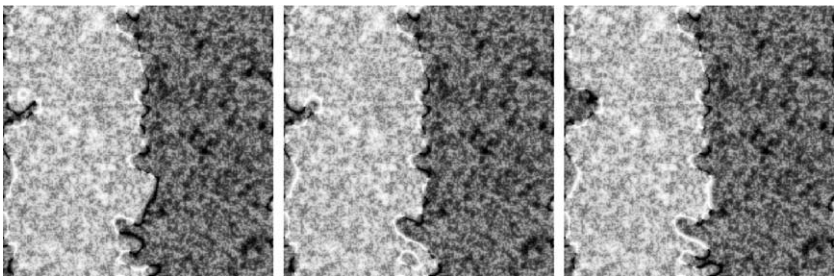

Fig. 10. Phase field of the 2:1 FCGL equation with $\gamma_1 = 0$, $\gamma_2 = 1$, $p = 0.62$, $\bar{\gamma} = 0.38$, $\ell = 1$, system size is 200×200, with periodic boundary conditions. Time increases from left to right in units of 1000 and results are shown after a transient time of $t_0 = 18\,000$ time units.

Fig. 10 shows dynamics for case (ii) from the same initial conditions. In contrast with case (i), the initial pattern has persisted apart from roughening of the initially planar fronts. Nearly all of the system is stationary, with the exception of some oscillatory motion at some places along the fronts. In case (ii), where some of the noise domains are forced below the phase-locking threshold, it may happen that small regions of the system exhibit oscillatory local dynamics and emit waves into the surrounding medium. However, the $\gamma(\mathbf{r})$ field for the realization shown in Fig. 10 does not contain any of these "pacemakers", a fact which was determined by performing a simulation with the spatially uniform initial condition $A(x, y, 0) \equiv A_0$. Hence, the time-varying behavior seen in Fig. 10 is a result of Bloch front reversal events. Note that in case (ii), no regions of the systems are being forced with values lying in the Bloch regime, yet Bloch-like front dynamics arise as a consequence of diffusive averaging.

5. Conclusions

The research described here shows that spatial inhomogeneities in the external forcing field can lead to a variety of types of wave propagation which result in both periodic

and irregular pattern formation dynamics in resonantly forced reaction–diffusion systems. In 2:1 resonantly locked systems the chemical patterns are associated with Bloch front reversals when an Ising domain is encountered. Situations of the sort considered in this paper, including both spatially regular and random forcing fields, can be realized in experiments on the periodically forced, light-sensitive Belousov–Zhabotinsky reaction which has been studied with spatially uniform forcing fields. In addition, similar phenomena should be seen if the spatial inhomogeneity exists in other system parameters and if spatially uniform periodic illumination is applied. Consequently, the phenomena described here could be found in naturally occurring oscillatory media, where inhomogeneity is the rule rather than the exception, subject to periodic forcing.

References

[1] V. Petrov, Q. Ouyang, H.L. Swinney, Nature 388 (1997) 655.
[2] V. Petrov, M. Gustaffson, H.L. Swinney, in: M. Ding, W. Ditto, L. Pecora, S. Vohra, M. Spano (Eds.), Proceedings of the Fourth Experimental Chaos Conference: August 6–8, 1997, Boca Raton, FL, USA, World Scientific, Singapore, 1998.
[3] A.L. Lin, V. Petrov, H.L. Swinney, A. Ardelea, G.F. Carey, in: M. Golubitsky, D. Luss, S.H. Strogatz (Eds.), Pattern Formation in Continuous and Coupled Systems; The IMA Volumes in Mathematics and Its Applications, Vol. 115, Springer, New York, 1999, p. 193.
[4] A.L. Lin, A. Hagberg, A. Ardelea, M. Bertram, H.L. Swinney, E. Meron, Phys. Rev. E 62 (2000) 3790.
[5] A. Yochelis, A. Hagberg, E. Meron, A.L. Lin, H.L. Swinney, "Development of standing-wave labyrinthine patterns", submitted to SIAM Journal on Applied Dynamical Systems (2001).
[6] C.J. Hemming, R. Kapral, Chaos 10 (2000) 731.
[7] J.M. Gambaudo, J. Differential Equations 57 (1985) 172.
[8] C. Elphick, G. Iooss, E. Tirapegui, Phys. Lett. A 120 (1987) 459.
[9] P. Coullet, K. Emilsson, Physica A 188 (1992) 190.
[10] T. Frisch, P. Coullet, J.M. Gilli, Phys, Rev. Lett. 72 (1994) 1471.
[11] D. Michaelis, U. Peschel, F. Lederer, D.V. Skyrabin, W.J. Firth, Phys. Rev. E 63 (2001) Article 066602.
[12] P. Coullet, J. Lega, B. Houchmanzadeh, J. Lajzerowicz, Phys. Rev. Lett. 65 (1990) 1352.
[13] P. Coullet, K. Emilsson, Physica D 62 (1992) 119.
[14] T. Kawagishi, T. Mizuguchi, M. Sano, Phys. Rev. Lett. 75 (1995) 3768.
[15] A. Hagberg, E. Meron, Nonlinearity 7 (1994) 805.
[16] C. Elphick, A. Hagberg, B.A. Malomed, E. Meron, Phys. Lett. A 230 (1997) 33.
[17] D. Haim, G. Li, Q. Ouyang, W.D. McCormick, H.L. Swinney, A. Hagberg, E. Meron, Phys. Rev. Lett. 77 (1996) 190.
[18] C. Elphick, A. Hagberg, E. Meron, Phys. Rev. E 51 (1995) 3052.
[19] A. Hagberg, E. Meron, Chaos 4 (1994) 477.
[20] A. Hagberg, E. Meron, I. Rubinstein, B. Zaltzmann, Phys. Rev. E 55 (1997) 4450.
[21] O. Steinbock, P. Kettunen, K. Showalter, Science 269 (1995) 1857.